4 Motion Planning in Deformable Soft Tissue with Obstacles with Applications to Needle Steering

In this chapter we introduce motion planning for *steerable needles*, a new class of needles that can follow curved paths around obstacles to reach clinical targets in soft tissue. Steerable needles are capable of reaching targets inaccessible by rigid needles.

We introduce a simulation and planner for steerable bevel-tip needle insertion that compensates for errors that occur due to tissue deformations. As in chapter 3, we begin with a simulation and planner in a 2-D imaging plane. Our interactive simulation approximates soft tissues as linearly elastic materials and uses a 2-D finite element model to compute tissue deformations due to tip and friction forces applied by the steerable needle. Polygonal obstacles represent tissues that cannot be cut by the needle, such as bone, or sensitive tissues that should not be damaged, such as nerves or arteries. The simulation enforces nonholonomic constraints on needle motion.

Our planner considers 4 degrees of freedom: initial location, initial orientation, binary bevel rotation, and insertion distance. The planner computes locally optimal values for these variables to compensate for tissue deformations and reach the target in simulation while avoiding polygonal obstacles and minimizing insertion distance so less tissue is damaged by the needle. Even in situations where real-time imaging such as ultrasound or interventional MRI is available, pre-planning is valuable to set the needle initial location and orientation and compute a desired trajectory that minimizes tissue damage.

4.1 Background on Needle Steering

Steerable needles follow curved paths when inserted into soft tissues. O'Leary et al. showed that needles with bevel tips bend more than symmetric-tip needles [170]. Webster et al. developed thin highly flexible bevel-tip needles using Nitinol and experimentally tested them in stiff tissue phantoms [208]. The needles followed constant-curvature paths in a plane when bevel rotation was fixed during needle insertion. Webster et al. [208] then developed a nonholonomic model for the steering flexible bevel-tip needles in rigid tissues. The nonholonomic model,

R. Alterovitz and K. Goldberg: Motion Planning in Medicine, STAR 50, pp. 45–55, 2008.
springerlink.com

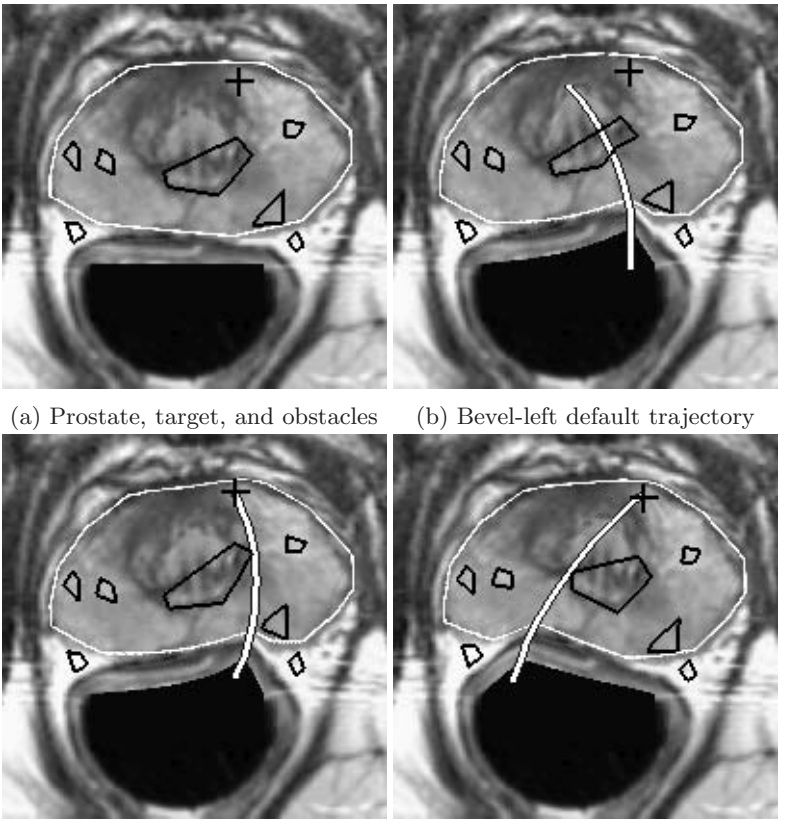

(a) Prostate, target, and obstacles (b) Bevel-left default trajectory

(c) Bevel-left plan (d) Bevel-right plan

Fig. 4.1. In this example based on an MR image of the prostate [121], a biopsy needle attached to a rigid rectal probe (black half-circle) is inserted into the prostate in simulation. Obstacles (polygons) and the target (cross) are overlaid on the image. The target is not accessible from the rigid probe by a straight line path without intersecting obstacles. However, bevel-tip needles bend as they are inserted into soft tissue (b). Our planner computes a locally optimal bevel-left needle insertion plan that reaches the target, avoids obstacles, and minimizes insertion distance (c). Using different initial conditions, our planner generates a plan for a bevel-right needle (d). Due to tissue deformation, the needle paths do not have constant curvature.

a generalization of a 3 degree-of-freedom bicycle model, was experimentally validated using a stiff tissue phantom.

Recent work has used a nonholonomic model of needle steering as a basis for motion planning in rigid tissues. Park et al. modeled 3-D needle steering using a unicycle model and used a diffusion-based method for planning without obstacles [171]. This work was based on advances by Zhou and Chirikjian in nonholonomic path planning, including stochastic model-based motion planning

to compensate for noise bias [224] and probabilistic models of dead-reckoning error in nonholonomic robots [223]. A more recent method for needle steering uses a screw-based model and optimization to compute locally optimal paths that avoid spherical obstacles in 3-D in seconds of computation time [75].

Past work has addressed steering symmetric-tip needles in 2-D deformable tissue that have 3 degrees of freedom: translating the needle base perpendicular to the insertion direction, rotating the the needle base along an axis perpendicular to the plane of the tissue, and translation along the needle insertion axis [72, 92]. DiMaio and Salcudean compute and invert a Jacobian matrix to translate and orient the base to avoid point obstacles with oval-shaped potential fields. Glozman and Shoham approximate the tissue using springs and also use an inverse kinematics approach to translate and orient the base every time step. In our work, we address bevel-tip steerable needles that have 2 degrees of freedom during insertion: rotation about the insertion axis and translation along the insertion axis.

4.2 Simulating Needle Steering

A bevel-tip needle, unlike a symmetric-tip needle, will exert asymmetric forces on the surrounding soft tissue when it is inserted. This causes the needle to cut tissue at an angle, as shown in figure 4.2. If the needle is sufficiently flexible, the asymmetric forces and angled cutting will cause the needle to bend in the direction of the bevel.

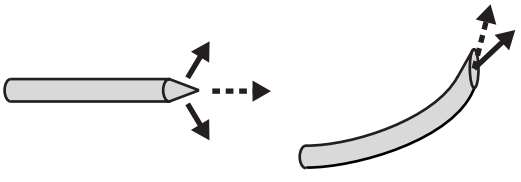

(a) Symmetric tip (b) Bevel tip

Fig. 4.2. A symmetric-tip needle (a) exerts forces (solid vectors) on the tissue equally in all directions, so it cuts tissue (dashed vector) in the direction that the tip is moving. A bevel-tip needle (b) exerts forces asymmetrically and cuts tissue at an angle.

In 2-D, we only consider 2 bevel rotations: bevel-right (0°) and bevel-left (180°), as shown in figure 4.1. Rotating the bevel to different orientations will cause the needle tip to move out of the imaging plane. In future work, we plan to extend our 2-D model to 3-D and consider any bevel orientation in the range [0°, 360°).

Our simulation models forces exerted by the needle on the soft tissue, including the cutting force at the needle tip and friction forces along the needle shaft. We assume needle bending forces are negligible compared to the elastic forces applied by the soft tissue to the needle.

4.2.1 Soft Tissue Model

We specify the anatomy geometry (i.e. the prostate and surrounding tissues) using a finite element mesh. The geometric input is a 2-D slice of tissue with tissue types segmented by polygons. We automatically generate a finite element mesh G composed of n nodes and m triangular elements in a regular right triangle mesh or using the constrained Delaunay triangulation software program Triangle [191], which generates meshes that conform to the segmented tissue type polygons.

The model must also include tissue material properties and boundary conditions for the finite element mesh. In our current implementation, we approximate soft tissues as linearly elastic, homogeneous, isotropic materials. For each segmented tissue type, the model requires tissue material properties (Young's modulus, Poisson's ratio, and density). We set values for these parameters as described in past work [18]. Mesh nodes inside bones are constrained to be fixed. A boundary condition of either free or fixed must be specified for each node on the mesh perimeter.

The complete tissue model M specifies the finite element mesh G, material properties, and boundary conditions. We assume the tissue in M is initially at equilibrium and ignore external forces not applied by the needle. We do not model physiological changes such as edema (tissue swelling), periodic tissue motion due to breathing or heart beat, or slip between tissue type boundaries.

4.2.2 Computing Soft Tissue Deformations

The *material mesh* G defines the geometry of the undeformed tissues, with each node i having coordinate $\mathbf{x}_i$ in the material frame. Forces resulting from needle insertion cause the tissue to deform. The deformation is defined by a displacement $\mathbf{u}_i$ for each node i in mesh G. The *deformed mesh* G' is constructed in the world frame using the displaced node coordinate $\mathbf{x}_i + \mathbf{u}_i$ for each node i. A point $\mathbf{y}$ in the material frame can be transformed to the world frame coordinate $\mathbf{y}'$ and vice versa using linear interpolation between the nodes of the enclosing finite element [17].

At each time step of the simulation we compute the acceleration of each node i, which includes acceleration due to elastic forces computed using a linear finite element method and the external force $\mathbf{f}_i$ exerted by the needle. We use explicit Euler time integration to integrate velocity and displacement for each free node for each time step. Time steps have duration $h = 0.01$ seconds.

4.2.3 Needle Insertion Model

Without loss of generality, we set the coordinate axes of the world frame so that the default needle insertion axis is along the positive z-axis. The y-axis corresponds to the initial location degree of freedom. The needle tip is initially located at a base coordinate $\mathbf{p}_0 = (y_0, z_0)$. The initial orientation of the needle is specified using θ, as shown in figure 4.3. For simulation stability, we constrain θ between $-45°$ and $45°$. The needle tip rotation is either bevel-right ($0°$) or bevel-left ($180°$). We assume the needle tip rotation is held constant during insertion

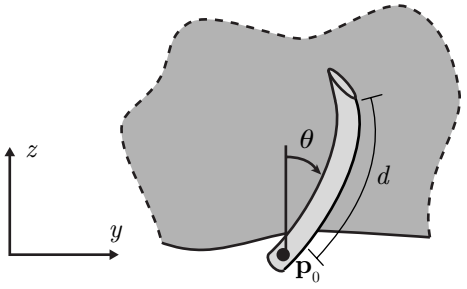

Fig. 4.3. Slice of soft tissue in the yz plane. The bevel-tip needle is initially at the base coordinate $\mathbf{p}_0$ with orientation θ. It is inserted a distance d, causing the surrounding soft tissue to deform.

due to planner efficiency and lack of experimental data for simulation, although we hope to relax this assumption in future work.

We assume the flexible needle is supported so that it does not bend outside the tissue. Once the needle has entered the tissue, it will bend in the direction of the bevel-tip. The distance the needle has been inserted from the base coordinate is d. We parameterize the needle by s where $s = 0$ corresponds the needle base and $s = d$ corresponds to the needle tip. Let $\mathbf{p}_s$ denote the material frame coordinate of the point along the needle a distance s from the base.

Simulation of needle insertion requires a needle model N that specifies needle properties, including insertion velocity v, the cutting force required at the needle tip to cut tissue, and the static and dynamic coefficients of friction between the tissue and needle.

We model the needle by line segment elements that correspond to edges of triangle elements in the deformed tissue mesh. Since the needle path is not known a priori, the material mesh must be modified in real-time. The simulation maintains a node at the needle tip location and a list of nodes along the needle shaft. At each simulation time step, the needle exerts force on the tissue at the needle tip, where the needle is displacing and cutting the tissue, and along the needle shaft due to friction.

Highly flexible bevel-tip needles tested in tissue phantoms by Webster et al. [208] were experimentally shown to follow a constant-curvature path when the bevel rotation was fixed during needle insertion. Setting simulation parameters to the limiting case of highly stiff tissue, zero tissue cutting force, and zero friction allows us to replicate this constant curvature path. In other cases, the needle path through deformed tissue may not be of constant curvature.

4.2.4 Simulating Cutting at the Needle Tip

During each simulation time step, the needle tip moves a distance vh in the world frame, where v is the needle insertion velocity and h is the time step

duration. The simulation must maintain element edges along the needle path, which requires mesh modification as the needle cuts through the tissue.

The simulation constrains a node to be located at the needle tip. The current needle tip node is labeled n_{tip} and the needle is pointed in direction $\mathbf{q}$. The needle will cut tissue a small distance d_{cut} along the vector $\mathbf{r}$ in the world frame, where $\mathbf{r}$ is deflected from $\mathbf{q}$ by an angle θ_d, as shown in figure 4.4. If the force at the needle tip along $\mathbf{r}$ is greater than a threshold f_{cut} based on needle and tissue properties, then the needle will cut through the tissue. Cutting is represented in the material mesh by moving the needle tip node n_{tip} by the distance d_{cut} transformed to the material frame. If no tissue deformation occurs, this method guarantees the needle will cut a path of constant curvature whose radius of curvature is a function of the deflection angle θ_d. When tissue deformation does occur at the needle tip, the path will be of constant curvature locally but will deviate from constant curvature globally depending on the magnitude of the deformations.

As the needle tip cuts through the mesh, it will be necessary to change the needle tip node. If the needle tip node is too close to the opposite triangle edge e, the tip node is moved back along the shaft and a new tip node, the closest node along edge e, is selected as the new tip node and moved to the new tip location in the material frame.

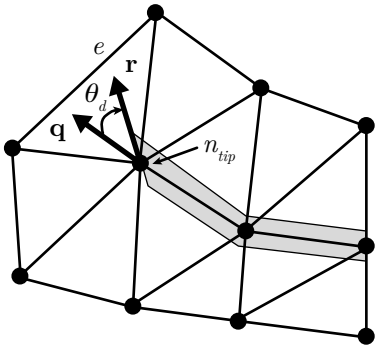

Fig. 4.4. The tissue mesh is modified so edge boundaries are formed along the path of needle insertion. A subset of the tissue mesh, centered at needle tip node n_{tip}, is shown. The straight line path of the needle is shown by vector $\mathbf{q}$. Because of the bevel-tip, the needle cuts tissue in direction $\mathbf{r}$, which is deflected from $\mathbf{q}$ by θ_d degrees.

4.2.5 Simulating Friction Along the Needle Shaft

We implemented a stick-slip friction model between the needle and the soft tissue. Nodes along the needle shaft carry friction state information; they are either attached to the needle (in the static friction state) or allowed to slide along the needle shaft (in the dynamic friction state).

When a node enters the static friction state, its distance from the needle tip along the shaft is computed. For each time step where the node remains in the static friction state, its position is modified by moving it tangent to the needle so that its distance from the tip along the needle shaft is held constant. A node moves from the static to the dynamic friction state when the force required to displace the node along the needle shaft exceeds a slip force parameter $f_{s_{max}}$.

When a node is in the dynamic friction state, a dissipative force is applied along the needle tangent. A node moves from the dynamic to the static friction state when the relative velocity of the needle to the tissue at the node is close to zero.

4.2.6 Simulation Results

Our simulator was implemented in C++ using OpenGL for visualization. It achieved an average of approximately 100 frames per second on a 1.6GHz Pentium M computer for a mesh composed of 1250 triangular elements. Computation time per frame increases linearly with the number of nodes along the needle shaft.

We demonstrate our simulation results in 2 cases: rigid tissue and deformable tissue. In both cases we simulate the insertion of a bevel-tip needle into a square of tissue fixed on 3 sides. In the first case, we consider tissue that is stiff relative to the needle and a sharp frictionless bevel-tip needle that cuts the tissue with zero cutting force. As shown in Fig 4.5(a), the simulated needle follows a path of constant curvature, which is the behavior experimentally verified by Webster et al. [208]. In the second case shown in figure 4.5(b), we insert the needle into a deformable soft tissue mesh with positive cutting force and friction coefficients.

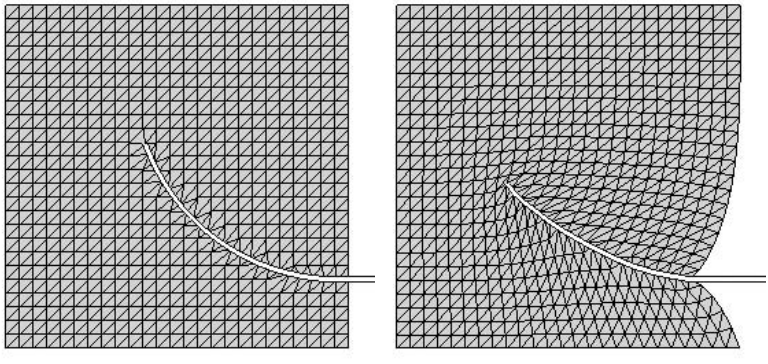

(a) Rigid Tissue (b) Deformable Tissue

Fig. 4.5. We simulate insertion of a bevel-tip needle into a square tissue fixed on 3 sides. When the tissue is stiff relative to the needle, a sharp frictionless needle cuts a path of constant curvature (a). A needle with positive cutting and friction forces will bend in deformable tissue (b).

Although the tip locally follows a path of constant curvature as explained in Section 4.2.4, the global path is not of constant curvature. Past experiments have demonstrated the effect of tissue deformations due to rigid needle insertion [17, 70]. We plan to develop experiments to test the bending behavior of flexible bevel-tip needles in deformable tissues to more accurately set parameters for our model in future work.

4.3 Motion Planning for Needle Steering

A needle steering plan is defined by $X = (y_0, \theta, b, d)$ where $y_0 \in \mathbb{R}$ is the insertion location, $\theta \in [-90°, 90°]$ is the insertion angle, $b \in \{0°, 180°\}$ is the bevel rotation, and $d \in \mathbb{R}^+$ is the distance the needle will be inserted. Obstacles are defined as non-overlapping polygons in a set O. The target is defined as a point $\mathbf{t}$ in the material frame of the soft tissue mesh. A plan X is feasible if the needle tip is within $\epsilon_t > 0$ of the target and the needle path in deformable tissue does not intersect any obstacle. The goal of needle insertion planning is to generate a feasible plan X that minimizes d.

4.3.1 Problem Formulation

The simulation of needle insertion described in Section 4.2 takes parameters X for the initial conditions and needle insertion distance, M for the soft tissue model, and N for the needle model and outputs the coordinates $\mathbf{p}_s$ for $s \in [0, d]$, which the needle will follow in the material frame.

$$\mathbf{p}_s = \text{NeedleSim}(X, M, N), s \in [0, d]$$

The variables of plan X are constrained by application specific limits y_{min}, y_{max}, θ_{min}, θ_{max}, and d_{max}.

$$\begin{aligned} y_{min} \leq y_0 \leq y_{max} \\ \theta_{min} \leq \theta \leq \theta_{max} \\ 0 \leq d \leq d_{max} \end{aligned}$$

These constraints enforce the limits of the simulation, such as the angle requirements in Section 4.2.3. In the biopsy example in figure 4.1, d_{max} is the maximum length of the needle and $y_{max} - y_{min}$ defines the width of the rectal probe.

The needle tip coordinate $\mathbf{p}_d$ in a feasible solution must be within Euclidean distance ϵ_t of the target $\mathbf{t}$.

$$\|\mathbf{p}_d - \mathbf{t}\| \leq \epsilon_t$$

In the presence of a nonempty set of polygonal obstacles O, we require that the needle path in a feasible solution does not intersect an obstacle. Let c_s be the distance from $\mathbf{p}_s$ to the closest point on the closest obstacle $o \in O$ and let the sign of c_s be negative if $\mathbf{p}_s$ is inside obstacle o and positive otherwise. We

require $c_s \geq \epsilon_o$ for some given tolerance $\epsilon_o \geq 0$ for all points s along the needle shaft. We formulate this constraint as

$$\int_0^d \max\{-c_s + \epsilon_o, 0\} ds \leq 0.$$

We can quickly compute this integral numerically using points sampled along the needle path.

We summarize the problem formulation for variable $X = (y_0, \theta, b, d)$ given target coordinate $\mathbf{t}$, polygonal obstacles O, tolerances ϵ_t and ϵ_o, tissue model parameters M, needle model parameters N, and variable limits y_{min}, y_{max}, θ_{min}, θ_{max}, and d_{max}.

$$\begin{aligned}
&\min f(X) = d \\
&\text{Subject to:} \\
&\quad \|\mathbf{p}_d - \mathbf{t}\| \leq \epsilon_t \\
&\quad \textstyle\int_0^d \max\{-c_s + \epsilon_o, 0\} ds \leq 0 \\
&\quad y_{min} \leq y_0 \leq y_{max} \\
&\quad \theta_{min} \leq \theta \leq \theta_{max} \\
&\quad 0 \leq d \leq d_{max}
\end{aligned}$$

The values of $\mathbf{p}_s$ for $s \in [0, d]$ are computed by executing the simulator NeedleSim(X, M, N). The obstacle distances c_s for $s \in [0, d]$ are computed using $\mathbf{p}_s$ and the set of obstacles O.

4.3.2 Optimization Method

To reduce the complexity of the optimization, we reduce the number of variables in X from 4 to 2. Given a plan X, we can find the optimal insertion distance d by executing the simulation to insertion distance d_{max} and identifying the point $\mathbf{p}_s$ along the needle path that minimizes the distance to the target $\mathbf{t}$. Hence, d does not need to be explicitly treated as a variable since its value is implied by the other variables in X. Furthermore, variable b in X is binary since it represents the bevel-right or bevel-left needle rotation state. We optimize X separately for the bevel-right and bevel-left states.

We solve for a locally optimal solution X^* using a penalty method. Penalty methods, originally developed in the 1950's and 1960's, solve a constrained nonlinear optimization problem by converting it to a series of unconstrained nonlinear optimization problems [31]. Given the constrained optimization problem $\min f(\mathbf{x})$ subject to $g(\mathbf{x}) \leq 0$, we can write the unconstrained problem $\min(f(\mathbf{x}) + \mu \max\{0, g(\mathbf{x})\}^2)$ for some large $\mu > 0$. Penalty methods generate a series of unconstrained optimization problems as $\mu \to \infty$. Each unconstrained optimization problem can be solved using Gradient Descent or variants of Newton's Method. For convex nonlinear problems, the method will generate points

that converge arbitrarily close to the global optimal solution [31]. For nonconvex problems, the method can only converge to a local optimal solution.

For steerable needle insertion planning, we convert the target and obstacle constraints to penalty functions to define a new nonlinear nonconvex optimization problem.

$$\min \hat{f}(X) = d + \mu \left(\max\{\|\mathbf{p}_d - \mathbf{t}\| - \epsilon_t, 0\}\right)^2 + \mu \left(\int_0^d \max\{-c_s + \epsilon_o, 0\} ds\right)^2$$

Subject to:

$$y_{min} \leq y_0 \leq y_{max}$$
$$\theta_{min} \leq \theta \leq \theta_{max}$$
$$0 \leq d \leq d_{max}$$

Evaluating the objective function $\hat{f}(X)$ requires executing the simulator NeedleSim(X, M, N) to compute the needle path $\mathbf{p}_s$ for $s \in [0, d]$ and the obstacles distances c_s. The remaining constraints are the limit constraints that are required for simulation stability and can never be violated.

We use Gradient Descent to find a local optimal solution to the unconstrained minimization problem $\min \hat{f}(X)$. The limit constraints are easily enforced at each iteration. We solve a sequence of 4 unconstrained problems, each with 10 Gradient Descent iterations. After each unconstrained problem has been solved, we multiply the penalty factor μ by 10. In future work, we plan to determine problem-specific termination criteria for the unconstrained optimization problems and for the penalty method.

The objective function $\hat{f}(X)$ cannot be directly differentiated since the simulator cannot be written as a closed form equation. For the Gradient Descent method, we numerically approximate the derivatives of the objective function with respect to the insertion location y_0 and orientation θ. We compute $d\hat{f}/dy_0$ by translating the needle path by Δy_0 and recomputing $\hat{f}$. Similarly, we compute $d\hat{f}/d\theta$ by rotating the needle path by $\Delta\theta$ about the insertion base coordinate $\mathbf{p}_0$ and recomputing $\hat{f}$. These approximations do not explicitly account for the different deformations that occur when y_0 or θ are modified but were sufficiently accurate for small Δy_0 and $\Delta\theta$ in our results described below.

4.3.3 Planner Results

We implemented the planner in C++ and used the simulation described in Section 4.2. Results for medical biopsy examples are shown in figure 4.1(c), figure 4.1(d), and figure 4.6(b). For each example, the tissue model mesh was composed of 1196 triangular elements and the planner required approximately 5 minutes of computation time on a Pentium M 1.6GHz computer. We set $\epsilon_t = \epsilon_o = 0.1$cm and the penalty method solution satisfied the constraints within a tolerance of 0.02.

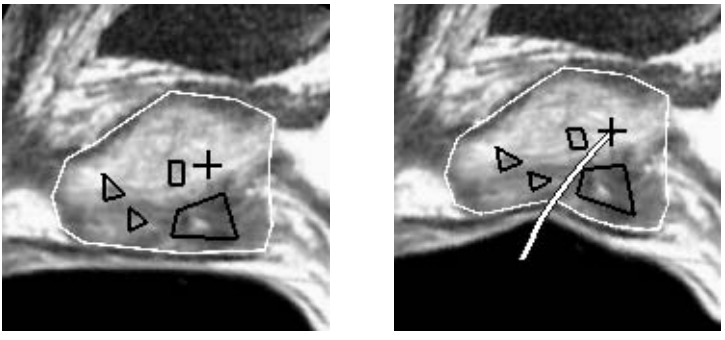

(a) Initial Conditions (b) Bevel-right Plan

Fig. 4.6. In this example based on an MR image of the sagittal plane of the prostate [121], a biopsy needle is inserted into the prostate (a). The planner computes an initial position, orientation, and insertion distance so the needle reaches the target (cross) while avoiding obstacles (polygons) and compensating for tissue deformations in simulation (b).

4.4 Conclusion and Open Problems

We described a needle insertion planning algorithm for steerable bevel-tip needles that combines numerical optimization with soft tissue simulation. The simulation, based on a linear finite element method described in chapter 2, is a generalization of the simulation of rigid needles introduced in chapter 3. The simulation models the effects of steerable needle tip and frictional forces on soft tissues defined by a 2-D mesh. Our planning algorithm computes a locally optimal initial location, orientation, and insertion distance for the needle to compensate for predicted tissue deformations and reach a target while avoiding polygonal obstacles.

The effectiveness of the planner is dependent on the accuracy of the simulation of steerable needle insertion and soft tissue deformations. Future work that would improve on these results includes comparing the output of our simulation to new physical experiments, determining the sensitivity of results to model parameters, allowing bevel rotation during insertion, and extending the simulation and planner to 3-D.